Int J Clin Exp Pathol 2017;10(5):6157-6169
www.ijcep.com /ISSN:1936-2625/IJCEP0052103

Original Article

DSTYK knockout affects the architecture of F-actin cytoskeleton in mouse renal proximal convoluted tubules

Ji-Wei Liu[1], Lin Mao[2], Zhi-Chuan Zhu[1], Kui Li[1], Lu-Jian Liao[2], Zhi-Qi Xiong[1], Ze-Lan Hu[1], Jing Zheng[1]

[1]Shanghai Key Laboratory of New Drug Design, School of Pharmacy, East China University of Science and Technology, Shanghai 200237, People's Republic of China; [2]School of Life Sciences, East China Normal University, Shanghai 200062, People's Republic of China

Received March 3, 2017; Accepted March 25, 2017; Epub May 1, 2017; Published May 15, 2017

Abstract: Mutations of dual serine/threonine and tyrosine protein kinase (*DSTYK*) are linked to congenital anomalies of the kidney and urinary tract (CAKUT). However, the function of DSTYK in the normal kidney and its role in the pathogenesis of CAKUT remain largely unknown. In this study, we investigated the role of DSTYK in the kidney by analyzing the consequences of *Dstyk* ablation in mice. We found that DSTYK deficiency resulted in swelling and diffuse distribution of F-actin cytoskeleton in proximal convoluted tubules. However, the architecture of F-actin cytoskeleton in the descending thin limb of Henel's loop, the thick ascending limb of Henel's loop, distal convoluted tubules, connecting tubules, collecting ducts and glomeruli was not affected following DSTYK deletion. The appearance of the urogenital system and the gross kidney anatomy of *Dstyk*$^{-/-}$ mice were normal. Also, no significant difference in the renal corpuscle's diameter and the density of glomeruli was found between *Dstyk*$^{+/+}$ and *Dstyk*$^{-/-}$ mice. To identify DSTYK binding partners, we generated a *Flag-DSTYK* knockin HEK 293T cell line with *Flag* tag sequence inserted to the N-terminus of endogenous *DSTYK* gene using CRISPR/Cas9 system. A total list of 67 proteins were identified by Co-immunoprecipitation (Co-IP)/mass spectrometry (MS) that potentially interact with DSTYK, mostly enzymes (39.0%), nucleic acid binding proteins (36.6%) and cytoskeletal proteins (14.6%). Profilin 1 and Profilin 2 were validated as bona fide DSTYK binding partners by Co-IP assay. These results uncover a role of DSTYK in the regulation of F-actin cytoskeleton in the mouse renal proximal convoluted tubules.

Keywords: DSTYK, CAKUT, F-actin, proximal convoluted tubules, Profilin 1, Profilin 2

Introduction

Congenital anomalies of the kidney and urinary tract (CAKUT), a broad range of disorders with malformations in the kidney and urinary tract, are the major causes of pediatric renal failure worldwide [1]. Despite the clinical importance, little is known about the molecular pathogenesis of these disorders. Familial cases account for about 10% of CAKUT patients [2], suggesting a genetic factor of CAKUT. A better understanding of genetic causes of CAKUT will forward our knowledge on the etiology of these diseases and facilitate early diagnosis of renal system abnormalities.

DSTYK (dual serine/threonine and tyrosine protein kinase, also known as RIP5) is a putative dual serine/threonine and tyrosine protein kinase which is ubiquitously expressed in vertebrates. Human *DSTYK* gene that localized in chromosome 1 encodes DSTYK protein comprising two non-catalytic regions and a catalytic kinase domain with unique structural features [3, 4]. *DSTYK* mRNA is expressed in multiple human tissues, such as brain, heart, kidney, lung and muscle [3]. Previously, whole-exome sequencing in combination with linkage analysis had identified *DSTYK* as a novel CAKUT-causing gene [5]. A heterozygous splice-site mutation (c.654+1G→A) of *DSTYK*, resulting in an in-frame deletion of nine amino acids (VTMHHALLQ) in exon 2, was detected in all seven affected members in a family with an autosomal dominant form of CAKUT. In addition, independent mutations of *DSTYK* gene

(including 1 nonsense, 1 splice-site and 3 missense mutations) were present in 2.3% of 311 unrelated CAKUT patients [5], suggesting that *DSTYK* is a susceptibility gene for CAKUT. It has been shown that DSTYK acts downstream of FGF signaling to regulate ERK phosphorylation [5, 6]. However, the role of DSTYK in the development and function of the kidney is still elusive.

In this study, we sought to investigate the biological role of DSTYK in the kidney using *Dstyk* knockout mice. Our results showed that *Dstyk* ablation perturbs the distribution of F-actin cytoskeleton in mouse renal proximal convoluted tubules (PCT), possibly through the actin-binding protein Profilin 1 and Profilin 2.

Materials and methods

Transgenic mice

The generation and genotyping of *Dstyk* knockout (*Dstyk*$^{-/-}$) mice were as previously described [7]. Animals were housed under standard conditions with regular light-dark cycle (12-h light/12-h dark) and free access to food and water. All animal experiments were carried out in accordance with the National Institutes of Health Guide for the Care and Use of Laboratory Animals.

Cell culture and transfection

Human embryonic kidney (HEK) 293T cells were maintained in Dulbecco's modified Eagle's medium (DMEM, Coring, Manassas, USA) supplemented with 10% fetal bovine serum (FBS, Gibco, Waltham, USA) under standard conditions at 37°C with 5% CO_2. Cells were transfected with Lipofectamine 2000 (Invitrogen, Carlsbad, USA) following the manufacturer's protocol.

Plasmids

Full-length coding sequences of *Profilin 1*, *Profilin 2* and *DSTYK* were amplified by PCR from a cDNA library of HEK 293T cells. The corresponding PCR products of *Profilin 1* and *Profilin 2* were ligated into pCAG-EGFP-N1 vector (constructed by replacing CMV promoter of Clontech pEGFP-N1 with CAG promoter), and PCR products of *DSTYK* was inserted into pCAG-tag2B vector (constructed by replacing CMV promoter of Stratagene pCMV-tag2B with CAG promoter).

Generation and genotyping of Flag-DSTYK knockin cell line

Single guide RNAs (sgRNAs) were designed using CRISPR Design Tool (http://crispr.mit.edu/, Zhang Feng Lab) and one sgRNA (sgRNA 1, 5'-GAGCGGGCAGAGGCGATGGAGGG-3') with relatively higher score and closer distance to the first codon of *Dstyk* gene was chosen. Corresponding oligos (forward: 5'-CACCGAGCGGGCAGAGGCGATGGA-3', and reverse: 5'-AAACTCCATCGCCTCTGCCCGCTC-3') were synthesized, annealed and ligated with BbsI linearized pX330-GFP vector (a gift from Dr. Hui Yang). The cleavage efficiency of sgRNA was assessed using SURVEYOR Mutation Detection Kit (Integrated DNA Technologies, Coralville, USA) following the manufacturer's protocol. A single-stranded DNA oligonucleotide (ssODN) was designed as donor repair template containing 60-bp homology arms flanking the site of alteration and purchased from Sangon Biotech (Shanghai, China) (ssODN sequence: 5'-AGGGAGGCCGGGCCTGCGGCCGGGGACCGAGCCGCAAAGACAGAGCGGGCAGAGGCGATGGATTACAAGGATGACGACGATAAGGAGGGCGACGGGGTGCCATGGGGCAGCGAGCCCGTCTCGGGTCCCGGCCCCGGCGGCGGC-3'). A mixture of 4 μg PX330-GFP-sgRNA1 plasmid and 4 μg donor ssODN were transfected into 60 mm dish-seeded HEK 293T cells. GFP-positive single cells were isolated through Fluorescence Activating Cell Sorter (FACS) and seeded into 96-well dishes 24 h later. After 2 weeks' expansion, clones were emerged and passaged. Genomic DNA of clones was extracted using TIANamp Genomic DNA kit (TIANGEN, Beijing, China), and genome around the targeted region was amplified with a set of primers (forward: 5'-ACACAAGAACGAGTGAGGGT-3', and reverse, 5'-CGGTCCGTCCTCCGATTTG-3') and then cloned into pGEM-T easy vectors (Promega, Madison, USA). After transformation into *E. coli* and extraction of plasmid DNA, Sanger sequencing was conducted to assess the targeted modification of each colony.

Real-time PCR

Total RNA was extracted from kidneys of adult *Dstyk*$^{+/+}$ and *Dstyk*$^{-/-}$ mice with Trizol reagent (Invitrogen, Carlsbad, USA). Complementary

DNA (cDNA) was then synthesized by iScript cDNA synthesis kit (Bio-Rad, Hercules, USA) and amplified using LightCycler 480 SYBR Green Master premix (Roche Diagnostics, Mannheim, Germany) following the manufacturer's protocol. For the amplification of mouse *Dstyk* partial cDNA, two pairs of primers were used: 5'-TGCCGCTTACCATGTTGAGG-3' and 5'-CACCCATGTGATACGCTGGAT-3' to amplify *Dstyk* exon 5-6; 5'-TGCTCATGTGCTAGCTGACC-3' and 5'-CCCGCTCAGAGAGTTCATCC-3' to amplify *Dstyk* exon 2-3. For amplifying mouse *Gapdh*, primers were 5'-TGGCAAAGTGGAGATTGT-3' and 5'-GTGGAGTCATACTGGAACA-3'.

Histology

Adult mice were sacrificed under anesthesia with pentobarbital sodium (70 mg/kg, i.p.) and perfused with 4% PFA/0.1 M PB. The kidneys were fixed in 4% PFA/0.1 M PB, cryoprotected in 30% sucrose/0.1 M PB and sectioned coronally at 40 μm intervals. H&E staining was carried out using a Hematoxylin and Eosin Staining Kit (Beyotime, Shanghai, China) according to the manufacturer's protocols, and images were taken by an upright microscope (Neurolucida, Nikon, Tokyo, Japan) with 10× air lens. The renal corpuscle's diameter of the renal cortex was measured by ImageJ software, and the number of glomeruli per millimeter of the renal cortex was calculated manually in every section observed.

Immunohistochemistry

40 μm sections of kidneys from adult *Dstyk*$^{+/+}$ and *Dstyk*$^{-/-}$ mice were blocked with blocking buffer (5% BSA, 0.3% Triton X-100 in PBS) for 1 h at room temperature and incubated with primary antibodies at 4°C overnight. Primary antibodies against the following proteins were used: rabbit anti-aquaporin 1 (AQP1) antibody (Millipore, Temecula, USA), goat anti-aquaporin 2 (AQP2) antibody (Santa Cruz Biotechnology, Dallas, USA), mouse anti-Calbindin D28K antibody (Sigma-Aldrich, St. Louis, USA) and mouse anti-NaKATPase α-1 antibody (Thermo Fisher Scientific, Rockford, USA). After washed in PBS for 3 times, sections were incubated with corresponding fluorescent secondary antibodies for 2 h at room temperature. F-actin was visualized by 0.1 μM tetramethylrhodamine B isothiocyanate (TRITC)-conjugated Phalloidin (Sigma-Aldrich, St. Louis, USA) diluted in blocking buffer according to the manufacturer's instructions. Nuclei were counterstained with Hochest (Beyotime, Shanghai, China). For analysis of fluorescence intensity, images were taken using an upright microscope (E80i, Nikon, Tokyo, Japan) with 10× air lens. The intensity of F-actin fluorescence was measured by ImageJ software, and all measured valves were corrected by subtracting the background obtained in a region of slide where no kidney tissue was present. For studying the distribution of F-actin cytoskeleton, z-stack confocal images were taken using a two-photon laser scanning microscope (A1R, Nikon, Tokyo, Japan) at 0.3 μm intervals with 60× oil lens.

Western blot

Kidney tissues from adult *Dstyk*$^{+/+}$ and *Dstyk*$^{-/-}$ mice were lysed in RIPA buffer (Beyotime, Shanghai, China) supplemented with 1 mM PMSF (Beyotime, Shanghai, China). Western blot was carried out as previously described [7]. Primary antibodies used were goat anti-DSTYK antibody (Santa Cruz Biotechnology, Dallas, USA) and HRP-conjugated anti-Actin antibody (Santa Cruz Biotechnology, Dallas, USA).

Co-immunoprecipitation (Co-IP)

For endogenous immunoprecipitation of lysates from clones 4 and 10, cells were lysed in IP buffer (20 mM Tris-HCl [PH 7.4], 150 mM NaCl, 1% Triton X-100, 1 mM EDTA, 1 mM EGTA and 10% glycerol) containing 1 mM NaF, 2 mM Na_3VO_4, 1 mM PMSF and 1× protease inhibitor cocktail (Sigma-Aldrich, St. Louis, USA) on ice for 20 min. The lysates were incubated with anti-FLAG M2 affinity agarose beads (Sigma-Aldrich, St. Louis, USA) at 4°C for 4 h, then the beads were collected by centrifugation and washed 3 times with IP buffer before subjected to mass spectrometry. For Co-immunoprecipitation of Flag and GFP fusion proteins, HEK 293T cells were transfected with indicated plasmids and harvested 24 h later. Cell lysis and immunoprecipitation were the same as endogenous immunoprecipitation. Precipitated proteins were eluted by loading buffer and boiled at 95°C for 5 min, then subjected to SDS-PAGE. Western blot was performed using rabbit anti-GFP (Thermo Fisher Scientific, Rockford, USA) and rabbit anti-Flag (Sigma-Aldrich, St. Louis, USA) antibodies.

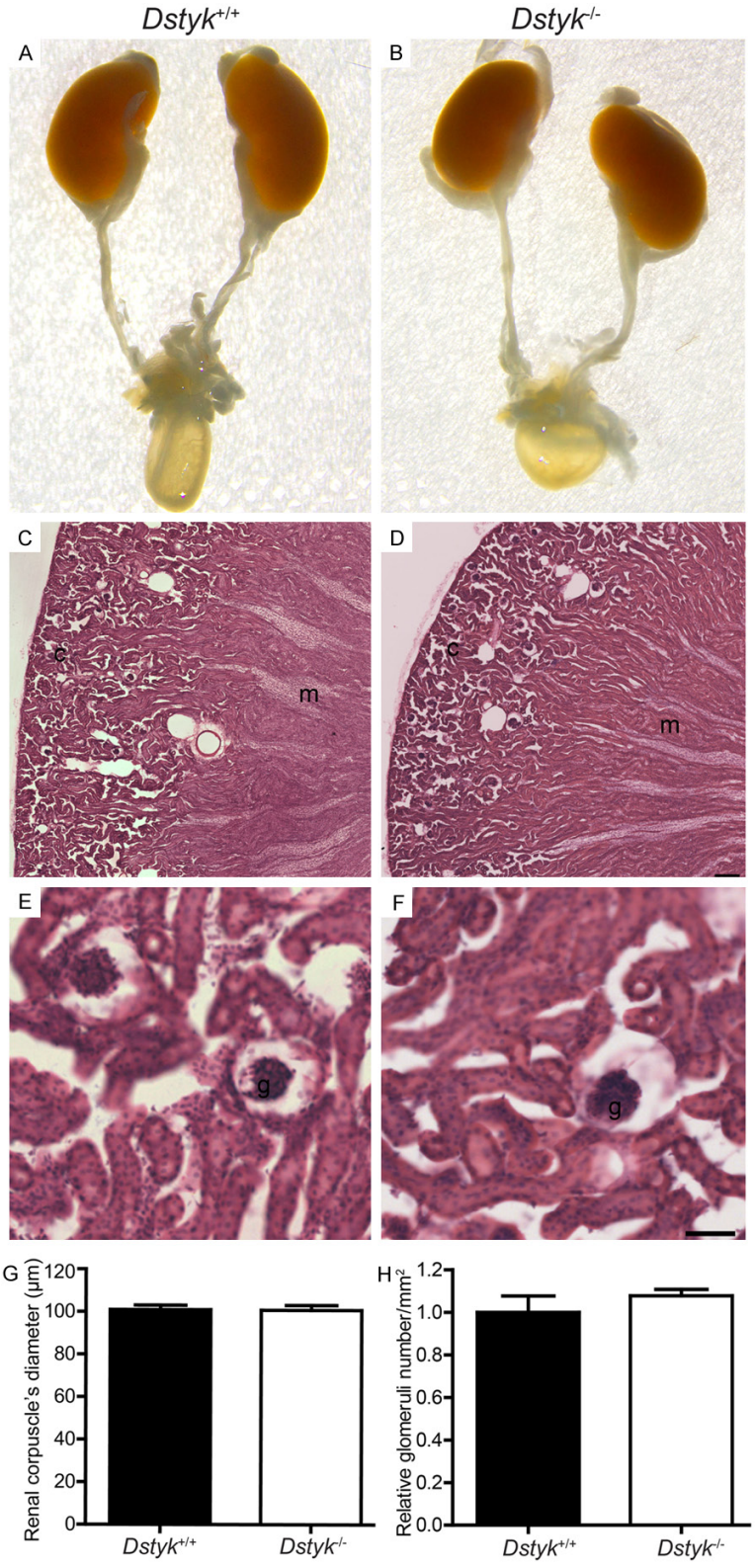

Figure 1. Gross appearance and histology of *Dstyk*$^{+/+}$ and *Dstyk*$^{-/-}$ kidneys. A and B. The overall appearance of urogenital systems from adult *Dstyk*$^{+/+}$ and *Dstyk*$^{-/-}$ mice. C and D. H&E staining; c, cortex; m, medulla; Bar, 200 μm. E and F. H&E staining; g, glomerulus; Bar, 50 μm. G. Statistical analysis of the renal corpuscle's diameter in *Dstyk*$^{+/+}$ and *Dstyk*$^{-/-}$ kidneys. Values are means ± SEM (n=3). H. Statistical analysis of the number of glomeruli per square millimeter in *Dstyk*$^{+/+}$ and *Dstyk*$^{-/-}$ kidneys. Values are means ± SEM (n=3).

Mass spectrometry (MS)

Lysates of clones 4 and 10 from three independent experiments were used to perform Co-IP/MS. Clone 10 was set as a negative control. After immunoprecipitation, beads were washed in PBS for 5 times, resuspended in 50 mM ammonium bicarbonate solution containing 8 M Urea, reduced with 10 mM DTT at 55°C for 30 min and alkylated with 15 mM iodoacetamide at room temperature in dark for 30 min. Proteins were digested with trypsin (Promega, Madison, USA) at 37°C for 16 h. The tryptic peptides were dried by vacuum centrifugation, extracted with 2% ACN/0.1% HAc and desalted using C-18 ZipTip (Millipore, Billerica, USA). Mass spectrometry was performed on a Q Exactive Mass Spectrometer (Thermo Fisher Scientific, Waltham, USA), and peptides were identified and scored using MaxQuant software.

Statistics

Data was analyzed by GraphPad Prism software and represented as mean ± standard error of the mean (SEM). Student's *t* test was used for statistical analysis of F-actin fluorescence and *p* values considered significant when $P<0.05$.

Results

Ablation of DSTYK expression in Dstyk$^{-/-}$ *kidneys*

To investigate the role of DSTYK in the kidney, we used a *Dstyk* knockout mouse strain, with exons 4-13 of *Dstyk* gene deleted [7]. Real-time PCR revealed that *Dstyk*$^{-/-}$ mice expressed truncated transcripts with comparable levels with full-length transcripts

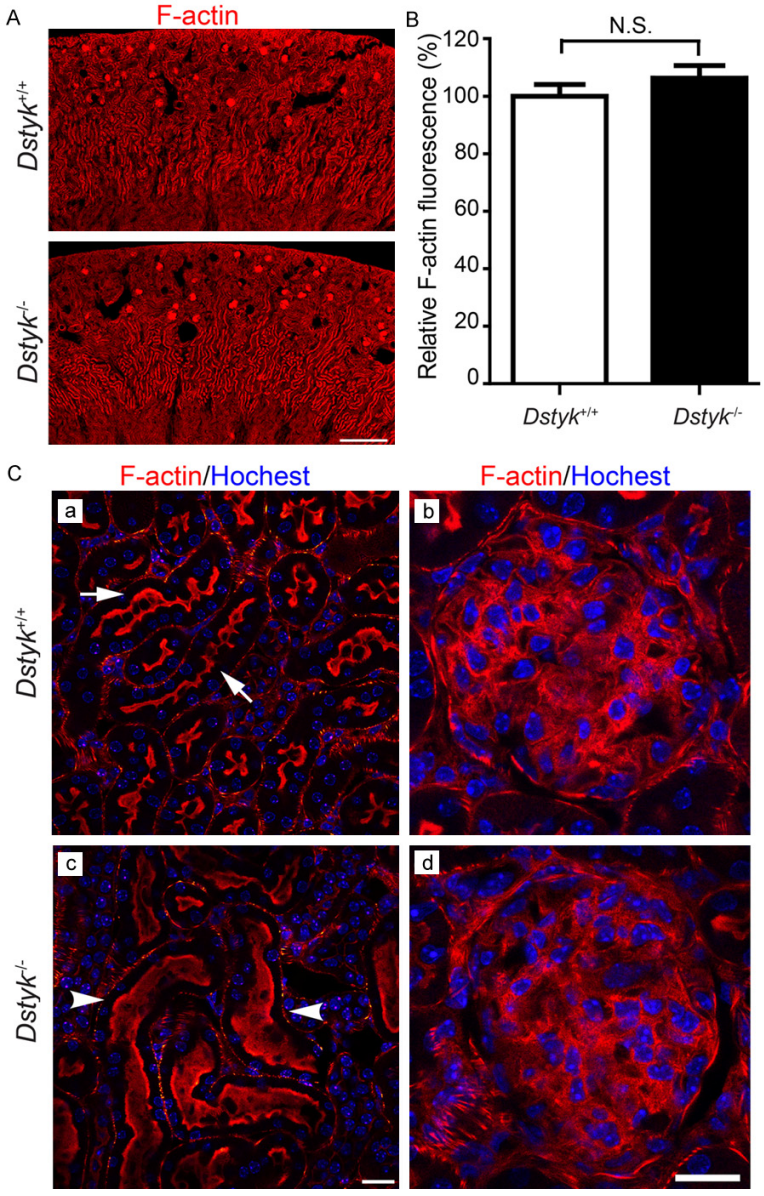

Figure 2. F-actin staining of kidneys from *Dstyk*$^{+/+}$ and *Dstyk*$^{-/-}$ mice. (A) The overall F-actin staining (red, phalloidin) of *Dstyk*$^{+/+}$ and *Dstyk*$^{-/-}$ kidneys; Bar, 500 μm. (B) Statistical analysis of F-actin fluorescence intensity of kidneys from *Dstyk*$^{+/+}$ and *Dstyk*$^{-/-}$ mice. Values are means ± SEM (n=3). N.S., not significant. (C) Confocal images of F-actin staining (red, phalloidin) in proximal convoluted tubules (a and c, characterized by the presence of apical brush-border membrane) and glomeruli (b and d). Arrowheads highlight the swelling and diffuse organization of the F-actin cytoskeleton in *Dstyk*$^{-/-}$ proximal convoluted tubules (c), in comparison with the compact and ordered cytoskeletal arrangement in controls (a, arrows). Nuclei were counterstained by Hochest. Scale bars, 20 μm.

expressed in control (*Dstyk*$^{+/+}$) mice (Figure S1A). By using an antibody against the N terminal of DSTYK protein, neither a full-length nor any low-molecular weight truncated DSTYK protein was observed in *Dstyk*$^{-/-}$ mice (Figure S1B), demonstrating the knockout of DSTYK protein in *Dstyk*$^{-/-}$ mice.

Normal overall appearance and histology of kidneys in Dstyk$^{-/-}$ *mice*

As previously described, *Dstyk*$^{-/-}$ mice were fertile and viable with no gross anatomical abnormality [7]. The overall appearance of urogenital systems and the size of kidneys from *Dstyk*$^{+/+}$ and *Dstyk*$^{-/-}$ mice were comparable (**Figure 1A** and **1B**). Histological examination after H&E staining showed that the gross morphology of the kidney (**Figure 1C** and **1D**) and the glomeruli (**Figure 1E** and **1F**) of *Dstyk*$^{-/-}$ mice appeared to be normal as compared with that of *Dstyk*$^{+/+}$ ones. No significant difference in the renal corpuscle's diameter and the density of cortical glomeruli was observed between *Dstyk*$^{+/+}$ and *Dstyk*$^{-/-}$ mice (**Figure 1G** and **1H**). These results suggest that the gross structure of kidney is undisturbed in *Dstyk*$^{-/-}$ mice.

Disrupted F-actin cytoskeleton organization in PCT of Dstyk$^{-/-}$ *mice*

Since changes of F-actin cytoskeleton may contribute to the pathophysiology of kidney disease [8, 9], we stained F-actin in *Dstyk*$^{+/+}$ and *Dstyk*$^{-/-}$ kidneys using TRITC-conjugated phalloidin. The overall staining pattern of F-actin and its fluorescence intensity were comparable between genotypes (**Figure 2A** and **2B**). However, in comparison with the compact and ordered F-actin cytoskeleton in PCT of *Dstyk*$^{+/+}$ mice, PCT of *Dstyk*$^{-/-}$ mice showed a more swelling and diffuse F-actin distribution. No alterations in

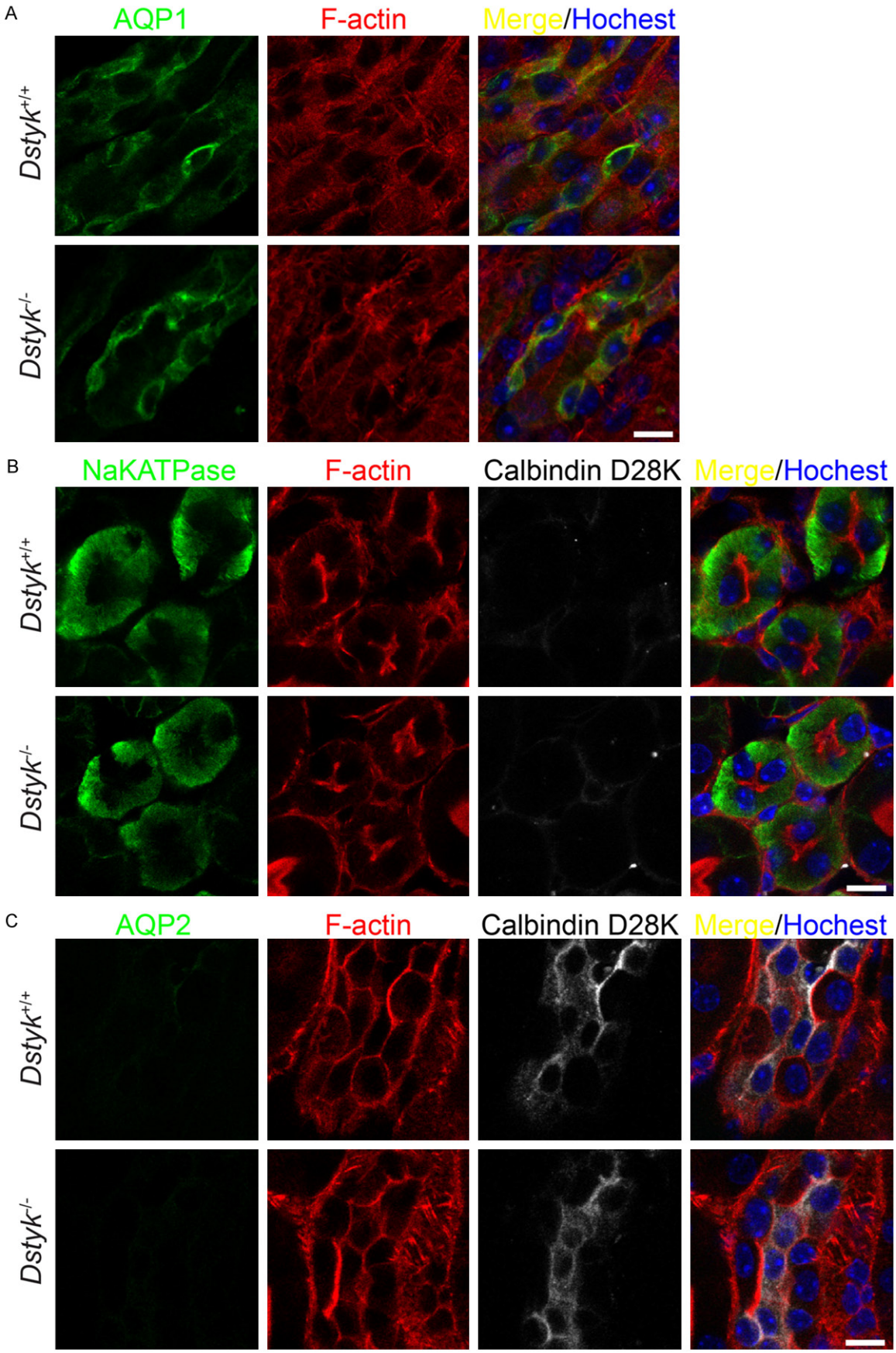
A
AQP1
F-actin
Merge/Hochest
Dstyk+/+
Dstyk-/-
B
NaKATPase
F-actin
Calbindin D28K
Merge/Hochest
Dstyk+/+
Dstyk-/-
C
AQP2
F-actin
Calbindin D28K
Merge/Hochest
Dstyk+/+
Dstyk-/-

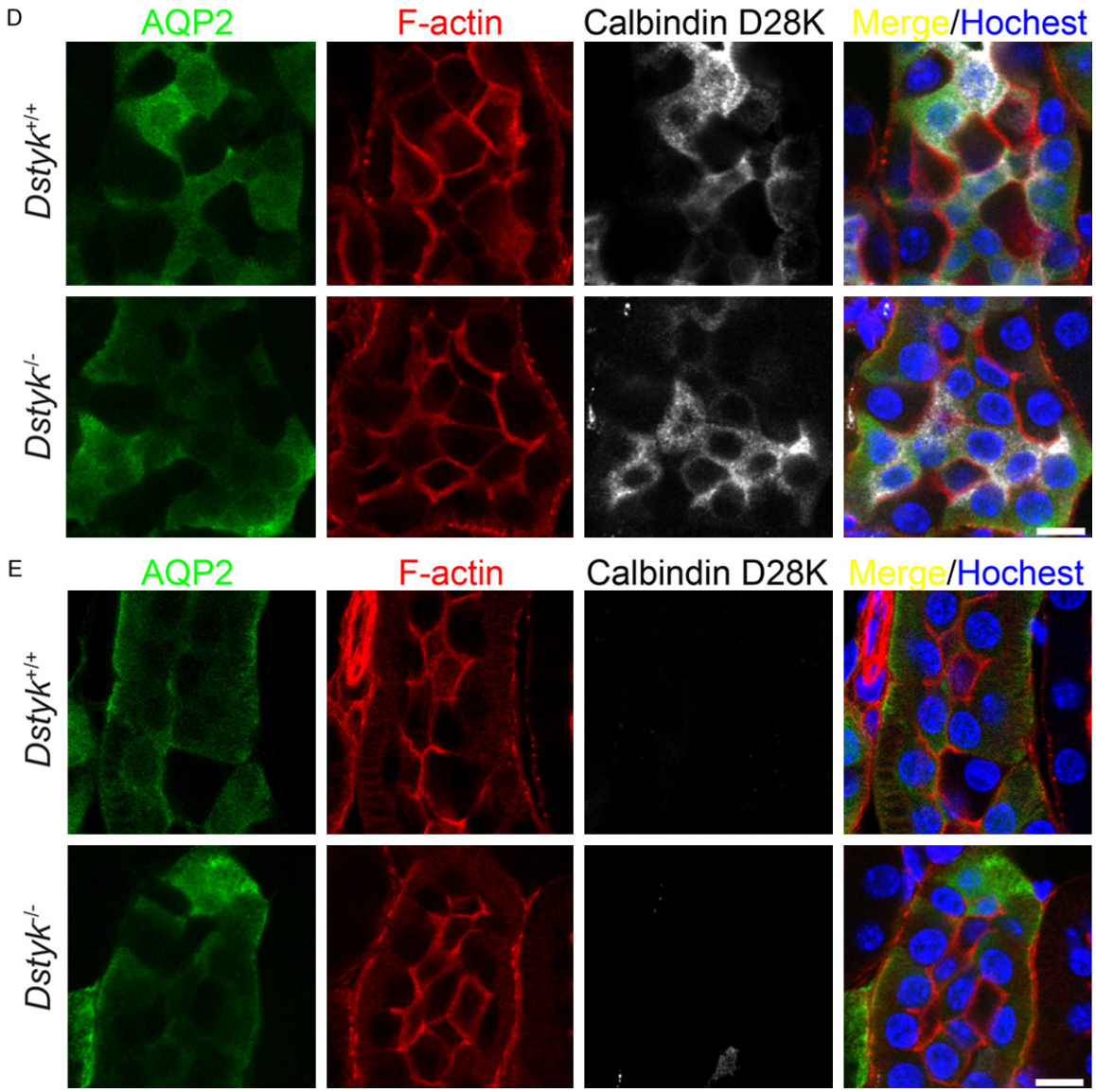

Figure 3. Distribution of F-actin cytoskeleton in nephron segments of *Dstyk*$^{+/+}$ and *Dstyk*$^{-/-}$ mice. Kidneys from adult *Dstyk*$^{+/+}$ and *Dstyk*$^{-/-}$ mice were stained against either AQP1 (A) or NaKATPase α-1 along with Calbindin D28K (B) or AQP2 together with Calbindin D28K (C-E), and costained with TRITC-conjugated phalloidin to visualize F-actin. Nuclei were counterstained by Hochest. Scale bars, 10 μm.

F-actin cytoskeleton of glomeruli was observed following DSTYK ablation (**Figure 2C**).

To further analyze the consequences of *Dstyk* ablation in the kidney, we used well-characterized segmental markers to label nephron segments. AQP1 has been reported to be expressed in PCT and descending thin limb [10, 11]. NaKATPase α-1 is expressed in thick ascending limb, distal convoluted tubules (DCT) and connecting tubules (CT) [11]. Calbindin D28K is a specific marker for DCT and CT [11, 12]. AQP-2 expression is restricted to CT and collecting ducts (CD) as previously reported [13, 14]. By co-staining these markers with TRITC-conjugated phalloidin, we didn't find the F-actin skeleton was disturbed in AQP1^{+} descending thin limb (**Figure 3A**), NaKATPase α-1^{+}/Calbindin D28K^{-} thick ascending limb (**Figure 3B**), Calbindin D28K^{+}/AQP2^{-} DCT (**Figure 3C**), Calbindin D28K^{+}/AQP2^{+} CT (**Figure 3D**) or Calbindin D28K^{-}/AQP2^{+} collecting ducts (CD) (**Figure 3E**) of *Dstyk*$^{-/-}$ mice. Together, these results demonstrate that *Dstyk* ablation affects the organiza-

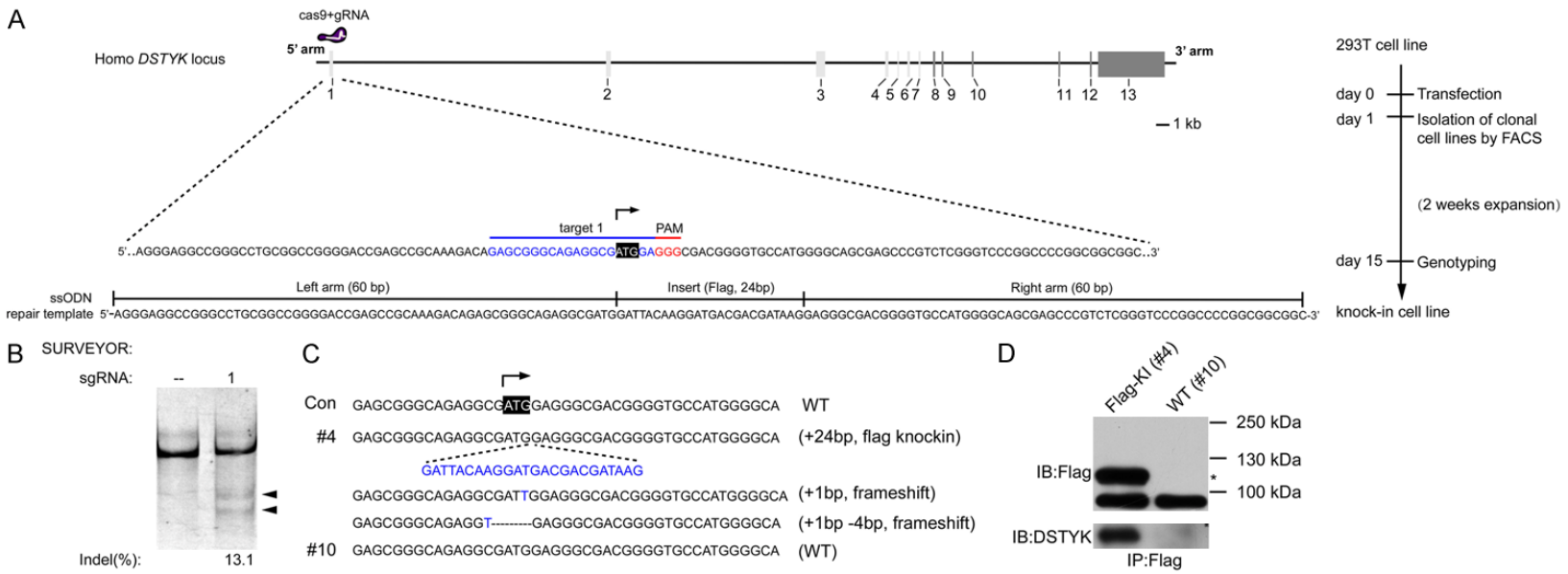

Figure 4. Generation of HEK 293T knockin cell line carrying *Flag* tag to the N terminus of *Dstyk* gene by CRISPR/Cas9 system. A. Schematic illustrating CRISPR/Cas9 system targeting human *Dstyk* locus and the experimental schedule. B. SURVEYOR assay showing on-target indel modifications of sgRNA 1. C. Cas9-mediated DNA mutations in #4 and #10 colonies. D. Immunoprecipitation using Flag antibody followed by Western blot confirmed the successful knockin of *Flag* tag in HEK 293T cell line. *indicates the band of Flag-DSTYK fusion protein.

Table 1. Potential DSTYK binding partners identified using Co-IP/MS in HEK 293T cells

Protein names	Gene names	Mol. Weight (kDa)	Sequence coverage (%)	Matched peptides	Score
Enzymes					
DDB1- and CUL4-associated factor 8	DCAF8	84.752	1.6	1	6.1502
RNA 3-terminal phosphate cyclase-like protein	RCL1	14.637	5.8	1	16.33
Cytoplasmic dynein 1 heavy chain 1	DYNC1H1	532.4	0.9	2	18.907
Poly (rC)-binding protein 1	PCBP1	37.497	11.2	2	23.506
ATP-citrate synthase	ACLY	91.098	1.8	1	7.0789
Guanine nucleotide-binding protein-like 3	GNL3	60.54	2.8	1	10.827
Putative ATP-dependent RNA helicase DHX30	DHX30	130.55	1	1	6.7039
Insulin-like growth factor 2 mRNA-binding protein 3	IGF2BP3	63.704	4.1	1	10.571
Cyclin-dependent kinase 2-associated protein 1	CDK2AP1	7.2241	19.7	1	7.0088
Thioredoxin domain-containing protein 12	TXNDC12	19.206	10.5	2	13.575
Peroxiredoxin-4	PRDX4	21.336	6.5	1	7.3244
Dolichol-phosphate mannosyltransferase subunit 1	DPM1	25.106	15.4	2	17.095
Enolase; Alpha-enolase	ENO1	21.02	5.1	1	9.2347
cAMP-dependent protein kinase catalytic subunit alpha	PRKACA	39.952	13.1	1	11.773
Nucleoside diphosphate kinase B	NME2	22.422	25.9	1	6.4778
ATPase family AAA domain-containing protein 3A	ATAD3A	64.243	3.3	2	60.087
Nucleic acid binding proteins					
DDB1- and CUL4-associated factor 8	DCAF8	84.752	1.6	1	6.1502
RNA 3-terminal phosphate cyclase-like protein	RCL1	14.637	5.8	1	16.33
FACT complex subunit SPT16	SUPT16H	7.5553	16.7	1	6.4509
Fragile X mental retardation protein 1	FMR1	34.114	4.7	1	7.2414
Poly (rC)-binding protein 1	PCBP1	37.497	11.2	2	23.506
Zinc finger CCCH-type antiviral protein 1	ZC3HAV1	114.08	1.3	1	6.074
Homer protein homolog 2	HOMER2	21.235	5.4	1	6.2637
Insulin-like growth factor 2 mRNA-binding protein 3	IGF2BP3	63.704	4.1	1	10.571
Cyclin-dependent kinase 2-associated protein 1	CDK2AP1	7.2241	19.7	1	7.0088
Homer protein homolog 1	HOMER1	20.819	12.8	2	15.801
26S protease regulatory subunit 4	PSMC1	41.167	3.3	1	8.3196
Reticulocalbin-1	RCN1	6.7524	27.6	1	8.4812
Methyl-CpG-binding domain protein 3	MBD3	26.322	6.4	1	6.6359
Transcription elongation factor A protein-like 4	TCEAL4	24.647	7.4	2	10.557
Putative 60S ribosomal protein L39-like 5	RPL39P5	6.3225	19.6	1	31.126
Cytoskeletal proteins					
Cytoplasmic dynein 1 heavy chain 1	DYNC1H1	532.4	0.9	2	18.907
28S ribosomal protein S35, mitochondrial	MRPS35	36.844	3.1	1	6.2824
Transmembrane protein 33	TMEM33	27.978	6.9	1	6.16
Tubulin beta-2A chain	TUBB2A	49.906	47.6	1	6.7379
Putative 60S ribosomal protein L39-like 5	RPL39P5	6.3225	19.6	1	31.126
Alpha-centractin	ACTR1A	34.557	5.3	1	19.749
Profilin-2	PFN2	9.7982	15.4	1	6.3051
Emerin	EMD	28.994	14.2	3	45.022
Transcription regulators					
Eukaryotic translation initiation factor 3 subunit E	EIF3E	26.635	11.5	2	16.814
Eukaryotic translation initiation factor 2 subunit 2	EIF2S2	38.388	3	1	8.9583
Eukaryotic translation initiation factor 1A, X-chromosomal	EIF1AX	13.232	8.6	1	7.2758
Antioxidants					
Peroxiredoxin-4	PRDX4	21.336	6.5	1	7.3244

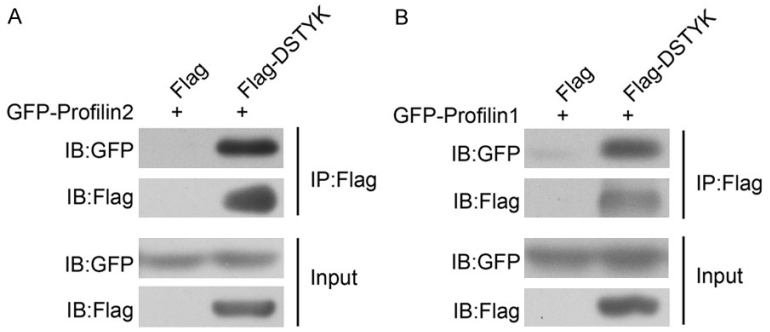

Figure 5. DSTYK interacts with Profilin 2 and Profilin 1. GFP-tagged Profilin 2 (A) and Profilin 1 (B) coimmunoprecipitated with Flag-DSTYK but not with the Flag control.

tion of F-actin cytoskeleton in PCT of the mouse kidney. However, the architecture of F-actin in glomeruli, descending thin limb, thick ascending limb, DCT, CT and CD was not altered following *Dstyk* ablation.

Searching for DSTYK binding partners

To further investigate the mechanism underlying the function of DSTYK in regulating F-actin cytoskeleton, Co-IP/MS were performed to identify DSTYK binding partners. First, we generated a knockin HEK 293T cell line carrying *Flag* tag to the N terminus of *Dstyk* gene using CRISPR/Cas9 system. In this system, we prepared a PX330-GFP cas9 expressing plasmid with a sgRNA sequence specifically target the human genome around the start codon of *DSTYK* gene and a single-stranded DNA oligonucleotide (ssODN) as donor repair template containing 60-bp homology arms flanking the site of alteration. The targeting strategies were illustrated in **Figure 4A**, and the sgRNA cleavage efficiency at targeted locus was verified by SURVEYOR assay (**Figure 4B**). Genotyping of isolated cell clones revealed that CRISPR/Cas9 system yielded targeted knockin in 4.2% of clones (1/24) and mutations in 66.7% of clones (16/24). For subsequent experiments, we used clones 4 (*Flag* knockin) and 10 (control) with sequences shown in **Figure 4C**. To assess whether *Flag-DSTYK* was expressed in knockin cells, we performed immunoprecipitation with FLAG M2 agarose beads followed by Western blot. Flag-DSTYK fusion protein was detected in lysates of clone 4 but not clone 10 by immunoblotting with either Flag or DSTYK antibody (**Figure 4D**).

Mass spectrometry analysis from three independent Co-IP experiments using FLAG M2 agarose beads and cell lysates from clones 4 and 10 identified 67 potential novel DTYK interaction partners. The identified proteins were grouped based on their known functions by the PANTHER classification system [15]. The most abundant were enzymes (39.0%), nucleic acid binding proteins (36.6%) and cytoskeletal proteins (14.6%) (Figure S2). The detected proteins involved in different cellular functions were presented in **Table 1**.

Profilin 1 and Profilin 2 interact with DSTYK in HEK 293T cells

Among the list of possible DSTYK interacting proteins, Profilin 2 is of particular interest because Profilins are small actin binding proteins which play an important role in F-actin polymerization and regulate the structure of F-actin [16, 17]. To determine whether Profilin 2 interacts with DSTYK, we co-expressed GFP-Profilin 2 with Flag-DSTYK or Flag in HEK 293T cells and performed a Co-IP assay using FLAG M2 agarose beads. The results revealed that GFP-Profilin 2 precipitated with Flag-DSTYK in co-transfected cells (**Figure 5A**). Since Profilin 1 shares greatest homology with Profilin 2 and is ubiquitously expressed in non-muscle cells [18], we also examined whether Profilin 1 interacts with DSTYK. Similarly, we found that GFP-Profilin 1 precipitated with Flag-DSTYK (**Figure 5B**). In both cases, as a negative control, Flag alone did not interact with GFP-Profilin 2 or GFP-Profilin 1.

Discussion

Congenital anomalies of the kidney and urinary tract (CAKUT) attribute to about 40-50% chronic renal failure in infants and children. Investigation the pathogenesis of CAKUT will improve therapies for early diagnosis and treatment of these disorders. Previously, several gene mutations had been shown to be responsible for human CAKUT, including *PAX2* (renal coloboma syndrome) [19], *KAL* (Kallmann syn-

drome) [20], *EYA1* (branchio-oto-renal syndrome) [21] and *HNF1β* (renal cysts and diabetes syndrome) [22]. By using whole-exome sequencing and linkage analysis, novel CAKUT-causing genes had been found (such as *DSTYK*, *TRAP1* and *TNXB*) [5, 23, 24], among which *DSTYK* is of particular interest since independent mutations of *DSTYK* had been found in 2.3% of unrelated CAKUT patients [5]. In this study, we found that *Dstyk*$^{-/-}$ PCT exhibited more disperse F-actin distribution, but *Dstyk*$^{-/-}$ descending thin limb of Henel's loop, ascending thick limb of Henel's loop, DCT, CT, CD and glomeruli appeared normal as compared with controls. This sparse distribution of F-actin network in *Dstyk*$^{-/-}$ PCT may be more vulnerable to deformation, with most of the forces exerted on only a small fraction of F-actin bundles [25]. Previous studies had shown that DSTYK protein was expressed in cell membranes of all tubular epithelia in postnatal mouse kidneys by immunohistochemistry [5]. Thus, *Dstyk* ablation may specifically affects the distribution of F-actin in mouse renal PCT. However, the expression pattern of *Dstyk* in the kidney still needs further validation due to the possibility of unspecific staining by antibodies.

F-actin cytoskeleton networks regulate cellular shape and support many aspects of cell physiology [26-28]. Disrupted integrity of F-actin cytoskeleton contributes to the pathogenesis of kidney diseases [8, 9]. The architecture of F-actin cytoskeleton is determined by both the polymerization dynamics of single actin filaments (rate of nucleation, growth and severing) and proteins facilitating the formation of F-actin secondary structures (crosslinking and bundling) [25, 29, 30]. Single actin filaments grow in a 'monomer treadmilling' model by adding ATP-globular actin to the 'plus' end and releasing ADP-globular actin from the 'minus' end [31], This dynamic process is regulated by monomer binding proteins, such as Profilin, Cofilin and CAP [16, 32]. In this study, we identified Profilin 1 and Profilin 2 as DSTYK interacting proteins. Thus, it is speculated that DSTYK may regulate F-actin cytoskeleton network through regulating the function of Profilin 1 and Profilin 2.

In summary, *Dstyk* knockout results in disrupted F-actin architecture in proximal convoluted tubule while sparing glomeruli and other major renal segments in mice. These results suggest that DSTYK modulates the distribution of F-actin cytoskeleton in proximal convoluted tubules and shed light on the mechanism underlying the pathogenesis of CAKUT contributed by DSTYK dysfunction.

Acknowledgements

Financial supports from the National Natural Science Foundation of China (Grant number 31300904) and the International Postdoctoral Exchange Fellowship Program (No.20130018) are acknowledged. We also thank professor Hui Yang for providing us with PX330-GFP plasmid.

Disclosure of conflict of interest

None.

Address correspondence to: Drs. Jing Zheng and Ze-Lan Hu, Shanghai Key Laboratory of New Drug Design, School of Pharmacy, East China University of Science and Technology, Shanghai 200237, People's Republic of China. Tel: 0086-21-64250608; Fax: 0086-21-64250608; E-mail: zhengjing@ecust.edu.cn (JZ); huzelan@hotmail.com (ZLH)

References

[1] Schedl A. Renal abnormalities and their developmental origin. Nat Rev Genet 2007; 8: 791-802.

[2] Winyard P and Chitty LS. Dysplastic kidneys. Semin Fetal Neonatal Med 2008; 13: 142-151.

[3] Peng J, Dong W, Chen Y, Mo R, Cheng JF, Hui CC, Mohandas N and Huang CH. Dusty protein kinases: primary structure, gene evolution, tissue specific expression and unique features of the catalytic domain. Biochim Biophys Acta 2006; 1759: 562-572.

[4] Zha J, Zhou Q, Xu LG, Chen D, Li L, Zhai Z and Shu HB. RIP5 is a RIP-homologous inducer of cell death. Biochem Biophys Res Commun 2004; 319: 298-303.

[5] Sanna-Cherchi S, Sampogna RV, Papeta N, Burgess KE, Nees SN, Perry BJ, Choi M, Bodria M, Liu Y, Weng PL, Lozanovski VJ, Verbitsky M, Lugani F, Sterken R, Paragas N, Caridi G, Carrea A, Dagnino M, Materna-Kiryluk A, Santamaria G, Murtas C, Ristoska-Bojkovska N, Izzi C, Kacak N, Bianco B, Giberti S, Gigante M, Piaggio G, Gesualdo L, Kosuljandic Vukic D, Vukojevic K, Saraga-Babic M, Saraga M, Gucev Z, Allegri L, Latos-Bielenska A, Casu D, State M, Scolari F, Ravazzolo R, Kiryluk K, Al-Awqati Q,

D'Agati VD, Drummond IA, Tasic V, Lifton RP, Ghiggeri GM and Gharavi AG. Mutations in DSTYK and dominant urinary tract malformations. N Engl J Med 2013; 369: 621-629.

[6] Lee JY, Hsu CK, Michael M, Nanda A, Liu L, McMillan JR, Pourreyron C, Takeichi T, Tolar J, Reid E, Hayday T, Blumen SC, Abu-Mouch S, Straussberg R, Basel-Vanagaite L, Barhum Y, Zouabi Y, Al-Ajmi H, Huang HY, Lin TC, Akiyama M, Lee JY, McLean WH, Simpson MA, Parsons M and McGrath JA. Large intragenic deletion in DSTYK underlies autosomal-recessive complicated spastic paraparesis, SPG23. Am J Hum Genet 2017; 100: 364-370.

[7] Li K, Liu JW, Zhu ZC, Wang HT, Zu Y, Liu YJ, Yang YH, Xiong ZQ, Shen X, Chen R, Zheng J and Hu ZL. DSTYK kinase domain ablation impaired the mice capabilities of learning and memory in water maze test. Int J Clin Exp Pathol 2014; 7: 6486-6492.

[8] Tian X and Ishibe S. Targeting the podocyte cytoskeleton: from pathogenesis to therapy in proteinuric kidney disease. Nephrol Dial Transplant 2016; 31: 1577-1583.

[9] Welsh GI and Saleem MA. The podocyte cytoskeleton--key to a functioning glomerulus in health and disease. Nat Rev Nephrol 2011; 8: 14-21.

[10] Kim WY, Lee HW, Han KH, Nam SA, Choi A, Kim YK and Kim J. Descending thin limb of the intermediate loop expresses both aquaporin 1 and urea transporter A2 in the mouse kidney. Histochem Cell Biol 2016; 146: 1-12.

[11] Tanaka M, Endo S, Okuda T, Economides AN, Valenzuela DM, Murphy AJ, Robertson E, Sakurai T, Fukatsu A, Yancopoulos GD, Kita T and Yanagita M. Expression of BMP-7 and USAG-1 (a BMP antagonist) in kidney development and injury. Kidney Int 2008; 73: 181-191.

[12] Georgas K, Rumballe B, Wilkinson L, Chiu HS, Lesieur E, Gilbert T and Little MH. Use of dual section mRNA in situ hybridisation/immunohistochemistry to clarify gene expression patterns during the early stages of nephron development in the embryo and in the mature nephron of the adult mouse kidney. Histochem Cell Biol 2008; 130: 927-942.

[13] Sasaki S, Fushimi K, Saito H, Saito F, Uchida S, Ishibashi K, Kuwahara M, Ikeuchi T, Inui K, Nakajima K, et al. Cloning, characterization, and chromosomal mapping of human aquaporin of collecting duct. J Clin Invest 1994; 93: 1250-1256.

[14] Takata K, Matsuzaki T, Tajika Y, Ablimit A and Hasegawa T. Localization and trafficking of aquaporin 2 in the kidney. Histochem Cell Biol 2008; 130: 197-209.

[15] Mi H, Muruganujan A, Casagrande JT and Thomas PD. Large-scale gene function analysis with the PANTHER classification system. Nat Protoc 2013; 8: 1551-1566.

[16] Revenu C, Athman R, Robine S and Louvard D. The co-workers of actin filaments: from cell structures to signals. Nat Rev Mol Cell Biol 2004; 5: 635-646.

[17] Dominguez R. Actin-binding proteins--a unifying hypothesis. Trends Biochem Sci 2004; 29: 572-578.

[18] Witke W, Podtelejnikov AV, Di Nardo A, Sutherland JD, Gurniak CB, Dotti C and Mann M. In mouse brain profilin I and profilin II associate with regulators of the endocytic pathway and actin assembly. EMBO J 1998; 17: 967-976.

[19] Sanyanusin P, Schimmenti LA, McNoe LA, Ward TA, Pierpont ME, Sullivan MJ, Dobyns WB and Eccles MR. Mutation of the PAX2 gene in a family with optic nerve colobomas, renal anomalies and vesicoureteral reflux. Nat Genet 1995; 9: 358-364.

[20] Oliveira LM, Seminara SB, Beranova M, Hayes FJ, Valkenburgh SB, Schipani E, Costa EM, Latronico AC, Crowley WF Jr and Vallejo M. The importance of autosomal genes in Kallmann syndrome: genotype-phenotype correlations and neuroendocrine characteristics. J Clin Endocrinol Metab 2001; 86: 1532-1538.

[21] Abdelhak S, Kalatzis V, Heilig R, Compain S, Samson D, Vincent C, Weil D, Cruaud C, Sahly I, Leibovici M, Bitner-Glindzicz M, Francis M, Lacombe D, Vigneron J, Charachon R, Boven K, Bedbeder P, Van Regemorter N, Weissenbach J and Petit C. A human homologue of the Drosophila eyes absent gene underlies branchio-oto-renal (BOR) syndrome and identifies a novel gene family. Nat Genet 1997; 15: 157-164.

[22] Lindner TH, Njolstad PR, Horikawa Y, Bostad L, Bell GI and Sovik O. A novel syndrome of diabetes mellitus, renal dysfunction and genital malformation associated with a partial deletion of the pseudo-POU domain of hepatocyte nuclear factor-1beta. Hum Mol Genet 1999; 8: 2001-2008.

[23] Saisawat P, Kohl S, Hilger AC, Hwang DY, Yung Gee H, Dworschak GC, Tasic V, Pennimpede T, Natarajan S, Sperry E, Matassa DS, Stajic N, Bogdanovic R, de Blaauw I, Marcelis CL, Wijers CH, Bartels E, Schmiedeke E, Schmidt D, Marzheuser S, Grasshoff-Derr S, Holland-Cunz S, Ludwig M, Nothen MM, Draaken M, Brosens E, Heij H, Tibboel D, Herrmann BG, Solomon BD, de Klein A, van Rooij IA, Esposito F, Reutter HM and Hildebrandt F. Whole-exome resequencing reveals recessive mutations in TRAP1 in individuals with CAKUT and VACTERL association. Kidney Int 2014; 85: 1310-1317.

[24] Gbadegesin RA, Brophy PD, Adeyemo A, Hall G, Gupta IR, Hains D, Bartkowiak B, Rabinovich

CE, Chandrasekharappa S, Homstad A, Westreich K, Wu G, Liu Y, Holanda D, Clarke J, Lavin P, Selim A, Miller S, Wiener JS, Ross SS, Foreman J, Rotimi C and Winn MP. TNXB mutations can cause vesicoureteral reflux. J Am Soc Nephrol 2013; 24: 1313-1322.

[25] De La Cruz EM and Gardel ML. Actin mechanics and fragmentation. J Biol Chem 2015; 290: 17137-44.

[26] Clarke M and Spudich JA. Nonmuscle contractile proteins: the role of actin and myosin in cell motility and shape determination. Annu Rev Biochem 1977; 46: 797-822.

[27] Pollard TD. Cytoskeletal functions of cytoplasmic contractile proteins. J Supramol Struct 1976; 5: 317-334.

[28] Stossel TP. Contractile proteins in cell structure and function. Annu Rev Med 1978; 29: 427-457.

[29] Falzone TT, Lenz M, Kovar DR and Gardel ML. Assembly kinetics determine the architecture of alpha-actinin crosslinked F-actin networks. Nat Commun 2012; 3: 861.

[30] Baum J, Papenfuss AT, Baum B, Speed TP and Cowman AF. Regulation of apicomplexan actin-based motility. Nat Rev Microbiol 2006; 4: 621-628.

[31] Carlier MF and Pantaloni D. Direct evidence for ADP-Pi-F-actin as the major intermediate in ATP-actin polymerization. Rate of dissociation of Pi from actin filaments. Biochemistry 1986; 25: 7789-7792.

[32] Baum B and Perrimon N. Spatial control of the actin cytoskeleton in Drosophila epithelial cells. Nat Cell Biol 2001; 3: 883-890.

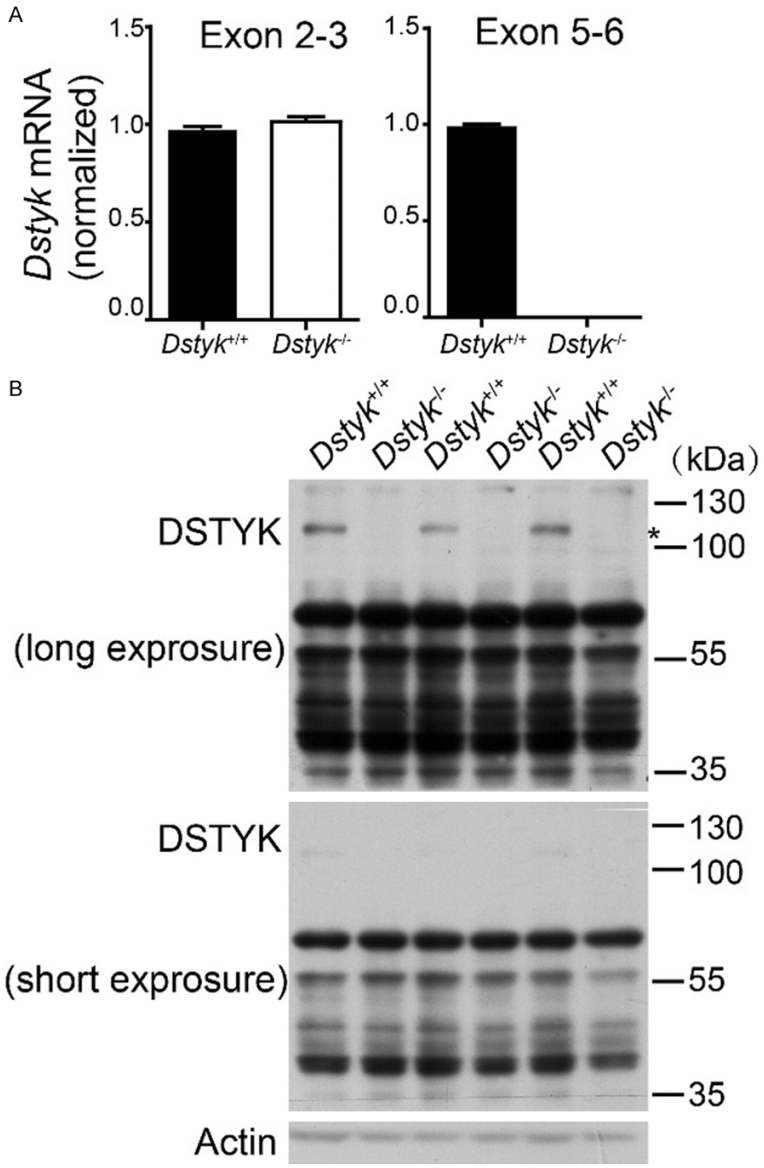

Figure S1. Ablation of DSTYK expression in kidney tissues of *Dstyk*$^{-/-}$ mice. A. Expression levels of *Dstyk* mRNA from kidney tissues of *Dstyk*$^{+/+}$ and *Dstyk*$^{-/-}$ mice was examined by Real-time PCR using primers amplifying both exon 2-3 and exon 5-6. Values (relative expression ratio to GAPDH) are means ± SEM (n=3). B. DSTYK protein levels in kidney lysates of *Dstyk*$^{+/+}$ and *Dstyk*$^{-/-}$ mice were analyzed by Western blot (n=3). Actin was used as a loading control. *indicates the band of DSTYK protein.

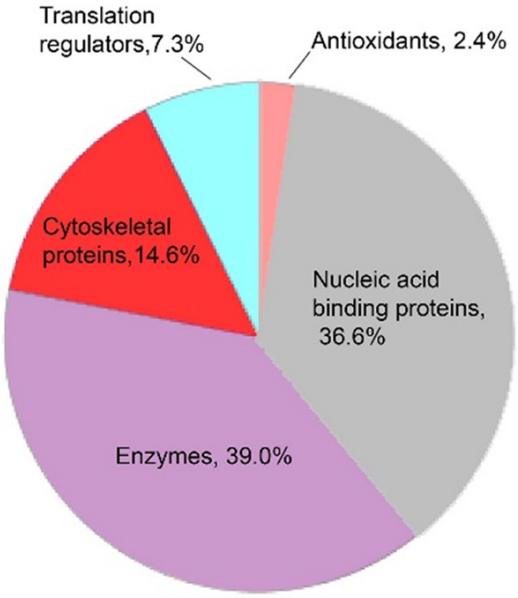

Figure S2. PANTHER analysis of proteins identified as potential DSTYK binding partners in HEK 293T cell line.